

pubs.acs.org/acsapm Article

Surfactant-Free Latex Nanocomposites Stabilized and Reinforced by Hydrophobically Functionalized Cellulose Nanocrystals

Yefei Zhang, Han Yang, Nevin Naren, and Stuart J. Rowan*



Cite This: ACS Appl. Polym. Mater. 2020, 2, 2291–2302



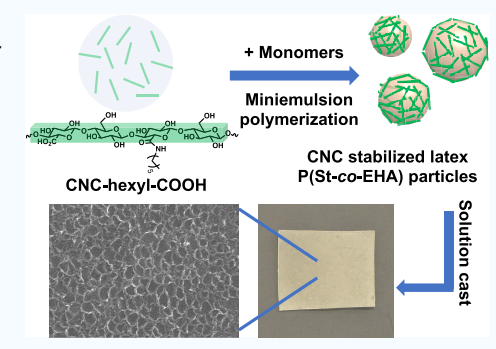
ACCESS

Metrics & More



Supporting Information

ABSTRACT: Stable poly(styrene-co-2-ethylhexyl acrylate) latex particles with diameter less than 600 nm were prepared by the miniemulsion polymerization of Pickering emulsions stabilized with hexyl-functionalized cellulose nanocrystals (CNC-hexyl-COOHs). Polymer nanocomposites were fabricated by casting of the CNC-stabilized latex particles, and the thermomechanical properties and microstructures of the films were studied and related to the type and amount of stabilizer as well as the processing conditions. Compared to the latex films stabilized with low-molecular-weight sodium dodecyl sulfate (SDS) surfactant, or using a combination of SDS and carboxylic acid CNC-COOHs, films stabilized solely with the alkyl-functionalized CNC-hexyl-COOHs showed much higher storage moduli in the rubbery regime and lower water uptake. Scanning electron microscopy (SEM) revealed a CNC network structure that is formed by excluded volume effects of the



latex particles, which concentrates the CNC-hexyl-COOHs into the interstitial space during solvent evaporation. This effect results in the formation of a percolation network at a lower CNC concentration within the latex composite films. The network can be further reinforced by increasing the concentration of CNCs through an "ex situ" process where CNC-hexyl-COOH-stabilized latex particles were mixed with CNC-COOH aqueous dispersions before film casting. The ability to replace low-molecular-weight surfactants in water-based latexes with alkyl-functionalized CNCs that are not only biosourced but also act as reinforcing agents offers an opportunity to expand the property profile of a variety of commercial products such as paints, coatings, and adhesives.

KEYWORDS: cellulose nanocrystals, nanocomposites, Pickering emulsions, emulsion templating, polymer latex particles, coatings

■ INTRODUCTION

Polymer latexes consist of microscopic polymer particles dispersed in a continuous liquid media (commonly water) and are used in a wide range of applications such as additives, cosmetics, adhesives, paints, and coatings.1 They can be formed by the polymerization of an emulsion, in which the noncontinuous phase contains monomers. If the latexes are composed of relatively low-glass-transition (T_{o}) (co)polymers, then it is possible to form a uniform film upon evaporation of the continuous phase.^{2,3} As such, water-based latexes have been studied and used extensively in commercial coating and adhesive products to replace solvent-based materials with the goal of reducing the environmental impact. However, latexbased coating films generally suffer from relatively low mechanical properties as a result of the low- T_{g} polymer in the formulation and the presence of the low-molecular-weight surfactant that is used to stabilize the emulsion/latex. One strategy that can be used to improve the performance of a latex film is the introduction of nanofillers into the latex dispersion, such as various inorganic nanoparticles (ZnO, TiO2, Al2O3, SiO₂),⁴⁻⁷ nanoclays,⁸ carbon nanotubes,⁹ as well as cellulose nanocrystals (CNCs). 10-14 These latex nanocomposites showed enhanced thermal, mechanical, and adhesive properties, which further broaden their applications in commercial products. 15

Among all of the potential nanofillers, cellulose nanocrystals (CNCs) have gained considerable attention for the preparation of more environmentally friendly polymer nanocomposites. CNCs are rodlike organic nanoparticles that can be isolated from a variety of renewable biosources through selective mechanical and chemical treatment. On account of their sustainability, excellent mechanical properties, and low density, CNCs have been widely explored as a green filler to reinforce a number of polymer matrices. The significant enhancement in the mechanical properties of the nanocomposites is attributed to the formation of a percolating CNC filler network within the polymer matrix through strong hydrogen-bonding interactions between the nanocrystals and/or between the nanocrystals to be uniformly dispersed within the polymer

Received: March 14, 2020 Accepted: May 11, 2020 Published: May 22, 2020





matrix, but it remains a challenge to mix unfunctionalized CNCs that are primarily hydrophilic with some hydrophobic polymers. The incompatibility between CNCs and such polymers can lead to phase separation and result in poor mechanical reinforcement.

To better disperse CNCs into a hydrophobic polymer matrix, nanocomposites can be prepared by mixing presynthesized polymer latexes with aqueous dispersions of CNCs, or by incorporating CNCs in situ during the polymerization to yield the latex, followed by casting and drying. Early work by Favier et al. showed that it was possible to access polymer nanocomposites by mixing aqueous suspensions of sulfuric acid-hydrolyzed tunicate CNCs with a commercial aqueous poly(styrene-co-butyl acrylate) latex stabilized with surfactants.²⁶ An increase in thermal stability and mechanical properties above the glass-transition temperature $T_{\rm g}$ was observed as a result of the incorporation of CNCs. ^{27,28} The effect of different processing methods on the mechanical properties of the latex-based nanocomposites has also been investigated in follow-up studies.^{29–33} For example, results showed that composites fabricated by casting, as opposed to freeze drying followed by melt processing, gave the highest mechanical reinforcement. 29-31 Similar results were observed in a study by Annamalai et al., where CNCs were added to a commercial low-molecular-weight surfactant-stabilized styrene-butadiene rubber (SBR) latex and the resulting CNCreinforced SBR composites prepared by casting demonstrated higher storage moduli than the composites prepared by compression molding.³³ The higher reinforcement observed in both works suggested that there is a different CNC network structure within the latex nanocomposites. It was hypothesized in both studies that the excluded volume of the latex particles concentrates all of the CNCs into the interstitial areas during water evaporation, which leads to the formation of a robust percolation network as well as a decrease in the percolation threshold relative to the case where CNCs are uniformly dispersed in the polymer matrix.32,33 However, no clear microscopic evidence for such CNC network structures was shown. Koning and co-workers reported the fabrication of conductive polymer nanocomposites by mixing poly(3,4ethylenedioxythiophene):poly(styrene sulfonate) (PE-DOT:PSS)-coated CNCs with presynthesized polystyrene (PS) latex particles that were stabilized with sodium dodecyl sulfate (SDS), and demonstrated that the percolation threshold of PEDOT:PSS conducting polymer decreased from 2.2 wt % to only 0.4 wt % with the addition of 0.8 wt % of CNCs.³⁴ The authors attributed the low threshold to the CNC network formed in the interstitial areas by PS latex templating effects, which were observed by scanning electron microscopy (SEM). More recently, Ballard and co-workers have shown that a honeycomb microstructure can be observed after mixing and drying negatively charged CNCs (length ca. 120 nm) with positively charged latex particles (size, 530 nm; stabilized with cationic surfactant) on account of electrostatic interactions and latex templating.³⁵ Such film structure leads to a significantly higher Young's modulus and ultimate tensile strength, consistent with the mechanical properties being heavily affected by the composite microstructure. It is worth pointing out that in the mixing approach to fabricate latex nanocomposites, low-molecular-weight surfactants are required to help stabilize the latex particles from aggregation. However, such surfactants are less favorable for film applications since they can lead to an increased sensitivity to water and a decrease

in gloss or adhesion properties by migrating to the interface or by forming aggregates. $^{36-38}\,$

As an alternative to the mixing approach utilized in these prior studies (which has been termed ex situ), composite films prepared from latexes that were synthesized with the CNCs present during the polymerization of the emulsion show enhanced mechanical properties. 10,11 This in situ method appears to promote better interactions between the CNCs and the polymer matrix through either better physical absorption or covalent grafting of the polymer from the surface of the CNCs. 39,40 The presence of CNCs at the interface also helps in stabilizing the monomer droplets by acting as a mechanical barrier to prevent particles from coalescing. In fact, it has been reported that sulfated CNCs can be used as solid stabilizers to access stable oil-in-water Pickering emulsions as a result of the amphiphilic character of the nanocrystals (one of the crystal faces (200) is hydrophobic). 41-47 However, to achieve nanosized emulsions with enhanced stability, covalent or noncovalent surface modification of CNCs is generally required. 48-57 Electrostatic interactions between charged surfactants and negatively charged CNCs have been shown to be an effective way to noncovalently modify the CNCs resulting in an enhanced wettability at the o/w interface. For example, Dubé and co-workers successfully synthesized CNC/ poly(n-butyl acrylate-co-methyl methacrylate) (P(BA-co-MMA)) latex nanocomposites for pressure-sensitive adhesive (PSA) applications using CNCs and the anionic surfactant sodium dodecyl sulfate (SDS) as co-stabilizers during emulsion polymerization. 58,59 They observed an improved mechanical performance (tack, peel strength, and shear strength) of the composite PSA films by increasing the CNC concentration from 0 to 1 wt %, and the level of reinforcement is better relative to nanocomposites prepared by simply mixing the CNCs with presynthesized P(BA-co-MMA) latex particles in water and drying (i.e., the ex situ approach).⁵⁹ The better reinforcement was attributed to the possible polymer grafting of the CNCs during in situ emulsion polymerization, as indicated by a high gel content of the nanocomposites (61.6 wt %). It is worth mentioning that in this case the latex interface will be stabilized by both the surfactant molecules and the CNCs. In another work reported by Boufi and co-workers, comonomers such as γ -methacryloxypropyl trimethoxysilane (MPS)^{14,60} and low-molecular-weight poly(ethylene glycol) methacrylate (MPEG)^{11,61} were added to the oil phase to facilitate the absorption of CNCs on the surface of the droplet during in situ polymerizations. A 2-fold increase in storage modulus in the rubbery regime and a 230% increase in adhesive strength of poly(vinyl acetate) nanocomposites (with 8 wt % of CNCs and 5 wt % of MPEG) were observed. 11 However, no details on how the microstructure of the composite films affected their properties were discussed.

Although the above research shows that hydrophobic polymers can be reinforced with CNCs through a latex approach, in most cases, low-molecular-weight surfactants are still required to help stabilize the formation of the nano emulsions. However, being surface-active, low-molecular-weight surfactants tend to migrate to the surface or to the substrate interface during the drying of the films. The aggregation of surfactants at the surface leads to leaching, discoloration of the coatings, and reduction in water resistance properties, barrier properties, and adhesion behavior. Therefore, it would be of interest to synthesize surfactant-free polymer latex composites that are stabilized only by function-

alized CNCs. Thus, the specific goal of this research is to build upon our prior work, which showed that alkyl-modified CNCs can be used to replace low-molecular-weight surfactants in o/w emulsions. 50 The alkyl-CNCs help to stabilize the emulsion by not only acting as Pickering stabilizers but also dropping the interfacial energy between the oil phase and the aqueous phase. However, these prior studies did not investigate how the use of these alkyl-CNCs as the only stabilizing agent affects film properties. Thus, reported herein is the preparation of lowmolecular-weight surfactant-free stable oil-in-water emulsions and latexes using styrene and 2-ethylhexyl acrylate (and 1 wt % methacrylic acid) as the oil phase and hexyl-modified CNCs as both the emulsion/latex stabilizer and reinforcing agent. Latex nanocomposite films were fabricated by simple casting from CNC-stabilized latex particle dispersions, and their mechanical properties and microstructures were investigated. The microstructures formed by in situ polymerization of the latexes stabilized with hexyl-modified CNCs were found to be critical to optimize mechanical reinforcement. In addition, these results are compared to the mechanical properties of lowmolecular-weight surfactant (in this case, sodium dodecyl sulfate, SDS)-stabilized latexes as well as SDS/CNC-stabilized latexes to evaluate the effect of removing the low-molecularweight surfactant on the properties of these latex films.

EXPERIMENTAL SECTION

Materials. Styrene and 2-ethylhexyl acrylate monomers were purchased from Sigma-Aldrich and purified by passing through a basic alumina-packed column to remove inhibitors. Methacrylic acid, (2,2,6,6-tetramethylpiperidin-1-yl)oxyl (TEMPO), sodium bromide (NaBr), sodium hypochlorite (NaOCl, 10-15 % available chlorine), sodium chlorite (NaClO₂), N-(3-dimethylaminopropyl)-N'-ethylcarbodiimide hydrochloride (EDC), N-hydroxysuccinimide (NHS), hexylamine, sodium metabisulfite, tert-butyl hydroperoxide solution (70% in H_2O), D-(-)-isoascorbic acid, sodium dodecyl sulfate (SDS), and dialysis membranes (14 kDa molecular weight cutoff) were all purchased from Sigma-Aldrich and used as received. Hydrochloric acid, glacial acetic acid, sodium hydroxide (NaOH), and potassium persulfate (KPS) were purchased from Fisher Scientific and used without further purification. Microcrystalline cellulose (MCC) (trade name: Lattice NT) was received from FMC Corporation (Newark, DE). Miscanthus x giganteus (MxG) stalks were donated by Aloterra Energy LLC (Conneaut, OH).

Synthesis of m-CNC-COOH via 2,2,6,6-Tetramethylpiperidin-1-yl)oxyl (TEMPO) Oxidation of MCC. Oxidation of MCC was performed using a previously published procedure. 50 MCC (5 g) was dispersed in 500 mL of DI water via sonication for 4 h using a Q500 QSonica ultrasonic processor at 40% amplitude. TEMPO (4 g, 25.6 mmol), NaBr (40 g, 388.7 mmol), and NaOCl (30 g, 403 mmol) were added into the dispersion while stirring. An additional NaOCl (10 g, 134.3 mmol) was added to maintain the pH of the reaction between 10 and 11. After the addition of NaOCl, 10 M NaOH was used to maintain the pH above 10. The pH of the solution was closely monitored, and the reaction was quenched by adding 25 mL of methanol when the pH stayed unchanged during a 15 min period. The CNC dispersion was centrifuged, and the supernatant was precipitated in excess methanol and collected via centrifugation. The product was further washed with methanol and DI water by successive centrifugation before being dialyzed against DI water for 2 days. Finally, m-CNC-COOH was recovered through lyophilization for 4 days using a VirTis BenchTop K lyophilizer.

Isolation and Oxidation of MxG-CNCs. MxG-CNC-OH was isolated from $Miscanthus\ x\ giganteus\ stalks$ and oxidized according to previously published methods. ⁶² Ground MxG powder (8 g) was soaked in 250 mL of a 2 wt % sodium hydroxide solution for 24 h. The base treatment was repeated twice in the same concentration of sodium hydroxide solution at 100 °C for 24 h. The solid was filtered

and washed thoroughly with DI water after each treatment. The remaining solid was redispersed into 180 mL of 2 wt % sodium chlorite solution with 12 mL of glacial acetic acid, and the dispersion was heated to 70 °C for 2 h under stirring before being filtered and washed. The white MxG pulp was further hydrolyzed in 100 mL of 1 M HCl solution at 75 °C for 15 h. The resulting pulp was thoroughly washed with DI water until neutral pH. The product was subjected to dialysis against DI water and collected via lyophilization. Hydrolyzed MxG-CNC-OH (1 g) was dispersed in 150 mL of DI water via ultrasonication before TEMPO (0.123 g), NaBr (1.23 g), and NaOCl (1.23 g) were added. The reaction was stirred at room temperature for 4.5 h, while the pH of the solution was maintained above 10 with the addition of 1 M NaOH solution. The reaction was quenched by adding excess methanol, and the oxidized product MxG-CNC-COOH was recovered as a white precipitate after centrifugation of the solution. Finally, the product was subjected to dialysis against DI water and collected via lyophilization.

Functionalization of CNCs with Hexylamine. m-CNC-COOH (1 g, 0.72 mmol of carboxylic acid moieties) was dispersed in 200 mL of dimethylformamide (DMF) via overnight sonication. EDC (0.60 g, 3.6 mmol, 5 equiv) was added, and the reaction was stirred for 5 min. Then, NHS (0.414 g, 3.6 mmol, 5 equiv) was added and the reaction was stirred for another 30 min. Hexylamine (0.364 g, 3.6 mmol, 5 equiv) was slowly added, and the reaction was stirred at room temperature for 16 h. The reaction was stopped by adding 100 mL of methanol, and the white precipitate was collected by centrifugation. The product was further washed with methanol (three times) and DI water (three times) under successive centrifugation, dialyzed against DI water, and finally lyophilized to yield m-CNC-hexyl-COOH. The same reaction was adopted on MxG-CNC-COOH (1 g, 0.92 mmol of carboxylic acid moieties) for the synthesis of MxG-CNC-hexyl-COOH. The Kaiser test was performed on the functionalized CNCs to ensure that free amine had been completely washed out.

Characterization of Hexyl-Functionalized CNCs. Conductometric Titration. The content of surface carboxylic groups of CNC-COOH and CNC-hexyl-COOH was determined through conductometric titrations. About 25 mg of CNC-COOH or 50 mg of CNChexyl-COOH was dispersed in 80 mL of DI water via overnight sonication in a Branson CPX sonication bath before titration. The pH of the dispersion was adjusted to below 3 by adding 15 μ L of concentrated HCl (33%), and the titration was performed by adding 0.01 M NaOH solution using an Accumet XL benchtop pH/ conductivity meter (Fisher Scientific). The conductivity was plotted against the volume of NaOH consumed, and the plateau region was used to determine the volume of NaOH used to neutralize the carboxylic acid groups, which can then be further used to calculate the content of carboxylic groups. The amount of hexyl groups was calculated by the difference in the number of carboxylic acid groups before and after functionalization.

Fourier Transform Infrared (FTIR) Spectroscopy. FTIR studies of CNCs were performed using a Shimadzu IRTracer-100 FTIR spectrometer. Freeze-dried CNC-hexyl-COOHs were placed directly on the attenuated total reflection (ATR) crystal, and the spectra were averaged from 45 scans between 400 and 4000 $\rm cm^{-1}$ with a resolution of 4 $\rm cm^{-1}$.

Atomic Force Microscopy (AFM). Suspensions of CNCs at a concentration of 0.01 wt % were drop-cast on freshly cleaved mica surfaces, which was pretreated with polylysine solutions. The samples were imaged using a Bruker Multimode 8 AFM instrument in the ScanAsyst mode. The AFM images were processed by Gwyddion software.

Emulsion and Latex Particle Preparation. *m*-CNC-hexyl-COOH or *MxG*-CNC-hexyl-COOH was dispersed in 7 g of DI water at desired concentrations (1, 2, and 3 wt % based on monomers) via ultrasonication. The monomer mixture (2 g), which consists of styrene, 2-ethylhexyl acrylate, and methacrylic acid at a weight ratio of 54:45:1, was added to the CNC/aqueous dispersion, and the resulting mixture was ultrasonicated (Branson Sonifier SFXS50) for 60 s under pulse mode (3 s on, 3 s off) to form an emulsion. The emulsion was purged with nitrogen for 10 min and

then sealed and heated up to 40 °C. Potassium persulfate (20 mg) and sodium metabisulfite (20 mg) were dissolved in 0.5 mL of DI water separately and injected dropwise as initiators. The polymerization was carried out at 40 °C for 2 h, and then the temperature was ramped up to 65 °C and left for 4 h. *tert*-Butyl hydroperoxide solution (2 mg, 70% aqueous solution) was diluted in 0.2 mL of DI water, added into the reaction, and stirred for 30 min. This was followed by the addition of 0.2 mL of D-(-)-isoascorbic acid aqueous solution (1 mg), and the polymerization was continued for another 30 min. Finally, the reaction was cooled down to room temperature.

Characterization of Latex Particles. Dynamic Light Scattering (DLS) and ζ (Zeta) Potential. The average diameter of the polymer latex particles was measured by dynamic light scattering. Samples were prepared by diluting 10 μ L of a latex particle suspension after polymerization in 2 mL of DI water. DLS, electrophoretic mobility, and ζ potential measurements were carried out simultaneously using a WYATT Mobiüs DLS detector.

Conversion. The conversion of the miniemulsion polymerization was measured gravimetrically. An aliquot of latex samples after polymerization was weighed, and the weight percent (wt %) of the polymer was calculated after drying the sample in a vacuum oven for 24 h at 100 °C. The conversion was calculated as the ratio between the wt % of polymer vs the theoretical wt % of monomer according to the formulation.

Latex Films Preparation. Solution Casting of Latex Films. Ascast latex films were prepared by directly casting the polymerized latex aqueous dispersion into poly(tetrafluoroethylene) (PTFE) dishes (diameter $\sim \! 10$ cm). Latexes were first dried in a fume hood for 24 h to evaporate most of the water and then dried at 90 °C in a vacuum oven for another 24 h to fully remove water and unreacted monomers. Homogeneous films with thickness between 200 and 300 nm were formed.

Melt Processing of Latex Films. The as-cast films were also compression-molded between two PTFE support films at 90 °C and 4000 psi for 10 min using a Carver laboratory press.

Characterization of Latex Films. Scanning Electron Microscopy (SEM). The cross section of the latex films was imaged by SEM. The films were first frozen in liquid nitrogen for 30 s and fractured to expose the cross-sectional areas. The fractured surfaces were then sputter-coated with 5 nm of Pd/Pt and imaged under a Carl Zeiss Merlin SEM.

Mechanical Properties. Latex films were cut into rectangular samples with an approximate dimension of 30 mm × 4 mm. The viscoelastic properties of the latex films were then analyzed using an RSA-G2 solid analyzer (TA Instruments, DE) equipped with a tension clamp. The modulus of the samples was analyzed using a temperature sweep method from -20 to 80 °C at a heating rate of 3 °C/min, with a fixed frequency of 1 Hz and a strain of 0.1%. All of the dynamic mechanical analyses (DMAs) were performed in triplicate, and the standard deviations were reported as error bars.

Swelling Test. Latex film samples were first weighed to obtain the dry mass before placing in vials filled with DI water. After 48 h, the samples were removed from water, gently blotted using a filter paper, and weighed to obtain the wet mass. The degree of water uptake can be calculated by

% swelling =
$$\frac{\text{wet mass} - \text{dry mass}}{\text{dry mass}} \times 100$$

RESULT AND DISCUSSION

Acrylate Emulsions and Latexes Stabilized by Hydrophobically Functionalized CNCs. In prior work, it has been shown that alkyl-modified CNCs better stabilize the o/w interface relative to carboxylic acid-functionalized CNCs. Therefore, carboxylic acid-functionalized CNCs from both microcrystalline cellulose (MCC) (*m*-CNC-COOH) and *M*. × giganteus (MxG-CNC-COOH) were functionalized with hexyl groups to increase the hydrophobicity of the nanocrystals.

Both m-CNC-COOH (length ~100 nm; height, 5.3 nm by AFM) and MxG-CNC-COOH (length ~300 nm; height, 3.4 nm by AFM) (Figure S1) were selected here with the goal of studying the effect of nanofiller aspect ratio on the mechanical reinforcement of the latex nanocomposites. The reaction of hexylamine with the CNC-COOHs using standard peptide coupling conditions (EDC/NHS) results in the formation of the hexyl functionalization CNCs (CNC-hexyl-COOH). FTIR spectra (Figure S2) of the oxidized CNC-COOHs show a peak at 1600 cm⁻¹, which is consistent with the formation of carboxylate moieties on the CNC surface. A new peak at 1645 cm⁻¹ showed up after hydrophobic modification, which is consistent with the formation of the amide bond, while the peak at 1720 cm⁻¹ corresponds to the carbonyl peak of the residual carboxylic acid moieties. The formation of the amide bond is further confirmed by an increase in the nitrogen content (0.75% for m-CNC-hexyl-COOH, 1.40% for MxG-CNC-hexyl-COOH), as determined by elemental analysis after functionalization (Table S1). Conductometric titrations showed that the carboxylic acid CNCs have surface carboxylic acid densities of 725 and 920 mmol/kg for m-CNC-COOH and MxG-CNC-COOH, respectively. After reaction with hexylamine, the residual carboxylic acid density dropped to ca. 270 mmol/kg for m-CNC-hexyl-COOH and to 360 mmol/ kg for MxG-CNC-hexyl-COOH, consistent with hexyl group densities of ca. 455 and 560 mmol/kg for m-CNC and MxG-CNC, respectively. This corresponds to CH₂/CH₃ (from the alkyl units)-to-COOH ratios of ca. 10.1 (m-CNC-hexyl-COOH) and 9.3 (MxG-CNC-hexyl-COOH), which are close the optimum ratio (ca. 9) that was found to give the smallest droplet sizes in the prior study.⁵⁰

A mixture of styrene, 2-ethylhexyl acrylate, and methacrylic acid at a weight ratio of 54:45:1 was employed as the oil phase with the goal of synthesizing low- $T_{\rm g}$ copolymer latexes that are similar to those used in water-based paints and coating applications (Scheme 1). The small percent of methacrylic acid was included in the monomer phase as it is commonly used in coating formulations to further aid latex stability. In this study, the oil/water ratio is kept at 20/80 (w/w) and the amount of hexyl-modified CNCs in the aqueous phase was varied

Scheme 1. Synthesis of Poly(styrene-co-2-ethylhexyl acrylate) Latex Particles via In Situ Miniemulsion Polymerization Stabilized Using CNC-Hexyl-COOH

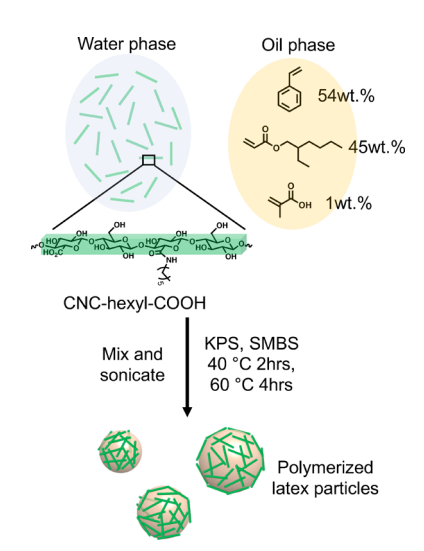


Table 1. Summary of the Poly(styrene-co-2-ethylhexyl acrylate) (P(St-co-EHA)) Latexes Stabilized with Different Types of Stabilizers^a

590.4 517.8	.7 \pm 5.8 82. .4 \pm 25.3 83. .8 \pm 16.1 86. .5 \pm 14.3 75.	7 -	$ -21.4 \pm 0.9 \\ -33.5 \pm 0.3 $
517.8	-8 ± 16.1 86.	.5	_
	_	-	-33.5 ± 0.3
490 9	5 + 143 75	5	
170.0	.5 _ 11.5	3	_
541.0	$.0 \pm 7.2$ 84		-28.5 ± 1.1
522.6	$.6 \pm 8.9$ 87.	.8	-33.0 ± 0.5
98.8	$.8 \pm 0.3$ 97.	.4	-21.6 ± 0.7
444.2	$.2 \pm 4.8$ 55.	.5	-38.1 ± 1.7
	$.3 \pm 4.8$ 53.	.3	_
		-	_

between 1, 2, and 3 wt % based on the mass of monomers. In addition, emulsions stabilized with MxG-CNC-COOH and/or low-molecular-weight surfactant SDS were prepared for comparison. Miniemulsion polymerization reactions were carried out with the different types and concentrations of stabilizers, and the properties of the final latex particles (sizes, conversion, ζ potential) are summarized in Table 1.

The poly(styrene-co-2-ethylhexyl acrylate) latexes stabilized by m-CNC-hexyl-COOH or MxG-CNC-hexyl-COOH at different concentrations are formed in good yield (>80%), except for the latex polymerized in the presence of 1 wt % of MxG-CNC-hexyl-COOH, which has a conversion of ca. 76%. A small amount of coagulation is observed, which decreases the overall yield of the stable emulsion, and is attributed to unoptimized stirring conditions in the small sample vials. The particle sizes of the latex stabilized with CNCs are all in the hundreds of nanometers range. While there is no clear correlation between the concentration of CNC-hexyl-COOH and particle size, the yield of latex obtained did increase with increasing CNC concentration. It is worth pointing out that the theoretical CNC coverage of the particles can be roughly estimated⁴² by the average size of the latex particles and the dimension of the CNCs assuming that all CNCs in the aqueous phase are absorbed at the interfaces (see Supporting Information (SI)). For m-CNC (h = 5.3 nm), the calculated coverages for the 1, 2, and 3 wt % latexes based on the average particle size from DLS are ca. 10, 27, and 34%, respectively, while the calculated coverages for the MxG-CNC (h = 3.4 nm) latexes are ca. 19, 38, and 53% (for 1, 2, and 3 wt %, respectively). The absorption of more CNCs at the surface of latex particles can be further demonstrated by their higher negative ζ potential with increasing CNC concentration, on account of the negatively charged COO ions on the surface of CNCs (Table S1). It should be noted that particularly at low CNC wt %, these coverage numbers are lower than that has been suggested to stabilize similar CNC-stabilized latex particles (ca. 40%). 42 The main difference here is the inclusion of 1 wt % methacrylic acid in the oil formulation, which presumably helps to stabilize the particles even at low CNC coverages. These results are consistent with the hexylfunctionalized CNCs acting as a stabilizer at the oil/water interface preventing significant coalescence during polymerization.

In the case where MxG-CNC-COOH was used as a stabilizer, the emulsion immediately showed phase separation after ultrasonication with a clear oil phase forming on top of the aqueous phase. Moreover, the latex was obtained in a relatively low yield (ca. 55%) after polymerization, which is

consistent with the reduced stability of the emulsion. Nonetheless, latex particles with an average size of ca. 440 nm are obtained, which are presumably stabilized by the negative charges from the methacrylate acid monomer and the decomposed persulfate (KPS) initiators.⁶³ To test this hypothesis, the same monomer mixture was mixed with water without using any surfactant (CNC or otherwise), and the emulsion showed the same phase separation behavior, particle size, and emulsion yield as observed with the MxG-CNC-COOH experiments. This result indicates that the size and stability of these methacrylic acid-containing latexes are not significantly affected by the presence of MxG-CNC-COOH. Taken together this data is consistent with the results from a previous study that shows that these alkyl-modified CNCs can reduce the interfacial tension between the oil and aqueous phases, while carboxylic acid CNCs have little to no effect on the interfacial energy. 50 It is important to note that the inclusion of the methacrylic acid monomer (1 wt %) and the use of persulfate initiator will help to prevent coalescence of the oil droplets, but the concentrations used in these experiments is not sufficient to stabilize the entire monomer phase, which is required to achieve high-yielding formation of the latex. Tuning the hydrophobic/hydrophilic balance of the CNCs (through reaction with hexylamine) allows the CNChexyl-COOHs to better stabilize the monomer/water interface and act as mechanical barriers to prevent further coalescence, which results in the formation of stable emulsions and latexes with an increase in yield of 20-30%. As a final control, an emulsion stabilized with a low-molecular-weight surfactant SDS was also polymerized and, as expected, resulted in much smaller particle sizes and higher conversion relative to the functionalized CNCs.

Mechanical Properties of Latex Films. Latexes stabilized with different concentrations of the hexyl-functionalized CNCs were cast from their water dispersions, to yield mechanically robust latex composite films after evaporation of the continuous phase. Figure 1 shows the images of the CNCstabilized latex nanocomposites at different loadings of CNCs. The films become less transparent as the concentration of nanocrystals increases from 1 to 3 wt % for both m-CNChexyl-COOH and MxG-CNC-hexyl-COOH. The temperature dependency of the storage modulus (E') of the latex nanocomposites containing various types and concentrations of stabilizers was measured by dynamic mechanical analysis (DMA) studies (Figure 2). The storage modulus (E') shows a transition between 20 and 40 °C, which is attributed to the glass transition of the P(St-co-EHA) matrix (glass-transition temperature, T_g , varied between 26 and 31 °C; Table 2). At

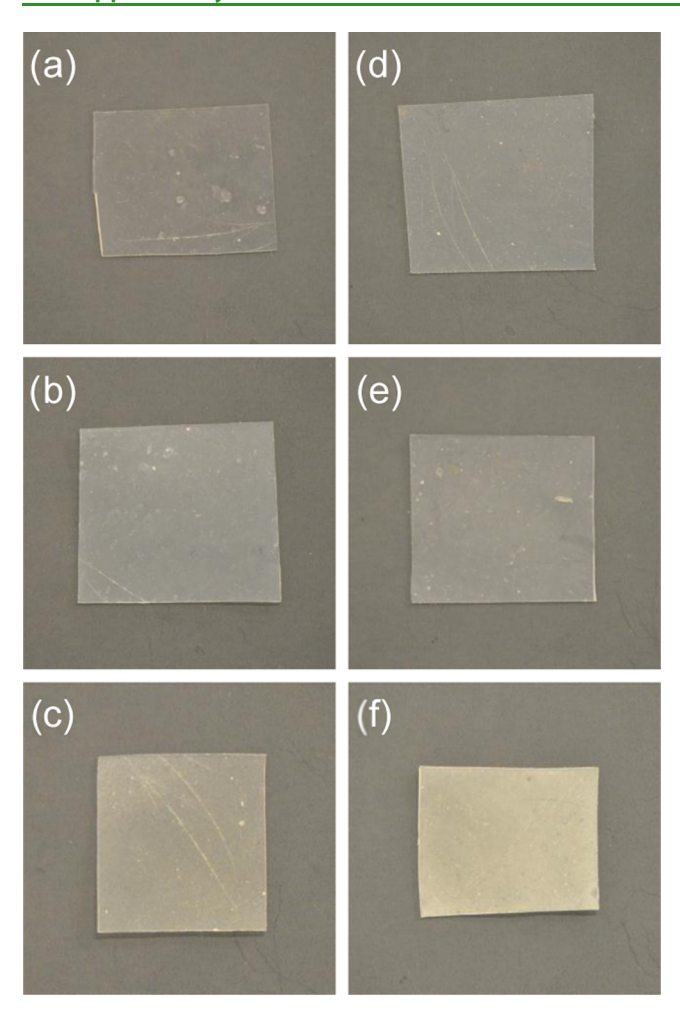


Figure 1. As-cast latex nanocomposites stabilized by (a) 1 wt %, (b) 2 wt %, and (c) 3 wt % of m-CNC-hexyl-COOH and by (d) 1 wt %, (e) 2 wt %, and (f) 3 wt % of MxG-CNC-hexyl-COOH (dimension of films: ca. 40 mm \times 40 mm).

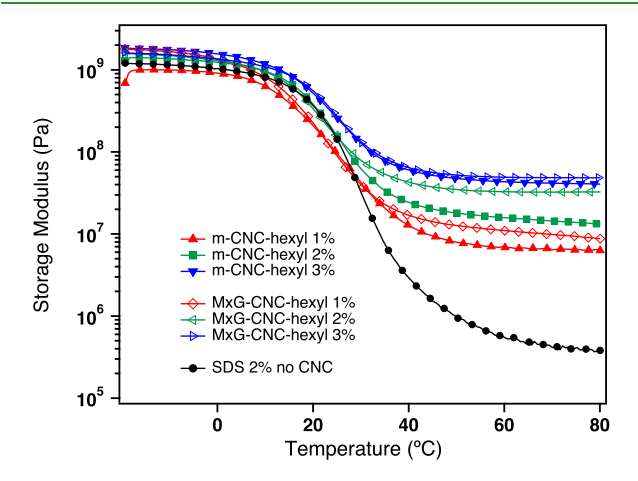


Figure 2. DMA temperature sweep study of the storage modulus (E') of the latex composite films stabilized with different types and concentrations of stabilizers (heating rate, 3 °C/min; frequency, 1 Hz; strain, 0.1 %). Loss modulus (E'') and $\tan \delta$ peak are shown in the SI (Figure S3).

temperatures lower than 20 $^{\circ}\mathrm{C}$ (i.e., below T_g), all latex films showed a similar storage modulus, regardless of the type and concentration of the stabilizers used, indicating that the

mechanical properties are dominated by the stiff polymer matrix. However, at temperatures above $T_{\rm g}$, the latex films containing the hexyl-functionalized CNCs exhibited a much higher plateau storage modulus relative to the latex films stabilized only with low-molecular-weight SDS surfactant. The plateau modulus also increases as the CNC concentration increases from 1 to 3 wt % for both m-CNC-hexyl-COOH-and MxG-CNC-hexyl-COOH-containing films. The mechanical reinforcement is consistent with the formation of a percolating CNC network akin to what has been reported in other CNC/polymer nanocomposites. 27,28,64

For latex composite films containing the same amount of alkyl-CNCs isolated from two different biosources, the plateau storage modulus is slightly higher for films stabilized with MxG-CNC-hexyl-COOH than for films stabilized with m-CNC-hexyl-COOH. The CNCs isolated from MCC have an aspect ratio of ca. 19, while MxG-CNCs have an aspect ratio of ca. 65.50,65 Therefore, the enhanced reinforcement effect of MxG-CNC-hexyl-COOHs may be attributed to the higher aspect ratio of the MxG nanocrystals, as predicted by the percolation model for fiber composites (see the Supporting Information).^{28,66} However, comparing the plateau modulus between the films containing alkyl-CNCs and SDS, the mechanical reinforcement effect by the alkyl-CNCs results in a modulus increase by up to 2 orders of magnitude (for 3 wt % MxG-CNC-hexyl-COOH). Even in the case when the amount of CNCs in the latex is less than the percolation threshold (as predicted by the aspect ratio of the filler), significant reinforcement is still observed. For example, the percolation threshold for the m-CNC is ca. 3.7 vol % (see Supporting Information for details), and as such no significant mechanical reinforcement is expected below 3.7 vol % (or ca. 5.4 wt % for the P(St-co-EHA) nanocomposites). However, the latex film stabilized with only 1 wt % of m-CNC-hexyl-COOH demonstrated a mechanical reinforcement with a storage modulus (E') of 7.0 \pm 0.2 MPa at 60 °C that is ca. 15 times higher than the storage modulus of SDS-stabilized latex film at the same temperature ($E' = 0.48 \pm 0.05$ MPa). Of course, the higher aspect ratio of MxG-CNCs means they have a lower percolation threshold (1.1 vol % or ca. 1.6 wt %) and the percolation model predicts a storage modulus at 60 °C of ca. 4.4 and 9.7 MPa for nanocomposites containing 2 and 3 wt % of MxG-CNC, respectively (see the Supporting Information for details). However, the MxG-CNC-hexyl-COOHs latex films show enhanced reinforcement relative to the model (E' = 25.9 ± 8.3 and 44.5 ± 4.1 MPa for 2 and 3 wt %, respectively), suggesting that there is something else going on other than a simple homogeneously distributed CNC network that is assumed in the model.

With the goal of better understanding this reinforcement effect, the internal microstructures of the latex nanocomposites were characterized by SEM (Figure 3). From the SEM images of the cross-sectional areas, a clear interconnected network structure can be observed within the films stabilized by either m-CNC and MxG-CNC. As the CNCs are predominately organized at the surface of the latex particles, the polymer particles act as an excluded volume, where no CNCs are present. The deformation of low- T_g latex particles concentrates the CNCs into the interstitial space between the particles, resulting in the formation of an interconnected network. It is important to note that given its dimensions, the "honeycomb" network observed in the SEM images presumably consists of a mixture of CNCs and polymer with the darker regions being

Table 2. Summary of the Storage Modulus (E') and Glass-Transition Temperature (T_g) of the Latex Composite Films Stabilized with Different Types and Concentrations of Stabilizers^a

stabilizer type	concentration (wt %)	as-cast		melt-pressed	
		E' at 60 °C (MPa)	T_{g}	E' at 60 °C (MPa)	$T_{ m g}$
m-CNC-hexyl-COOH	1	7.0 ± 0.2	30.5	1.0 ± 0.1	31.5
m-CNC-hexyl-COOH	2	17.1 ± 1.7	28	1.2 ± 0.1	31.4
m-CNC-hexyl-COOH	3	32.9 ± 10.8	28.3	1.5 ± 0.4	31.8
MxG-CNC-hexyl-COOH	1	14.5 ± 2.4	27	1.0 ± 0.1	28.4
MxG-CNC-hexyl-COOH	2	25.9 ± 8.3	26.3	1.5 ± 0.1	30.3
MxG-CNC-hexyl-COOH	3	44.5 ± 4.1	27.9	2.2 ± 0.3	33.2
SDS	2	0.48 ± 0.05	29.5	0.76	32.6
m-CNC-COOH/SDS	2	11.1 ± 1.8	29.1		
MxG-CNC-COOH/SDS	2	12.7 ± 1.6	30.8		

 $^{{}^}aT_{\rm g}$ determined from the peak of tan δ .

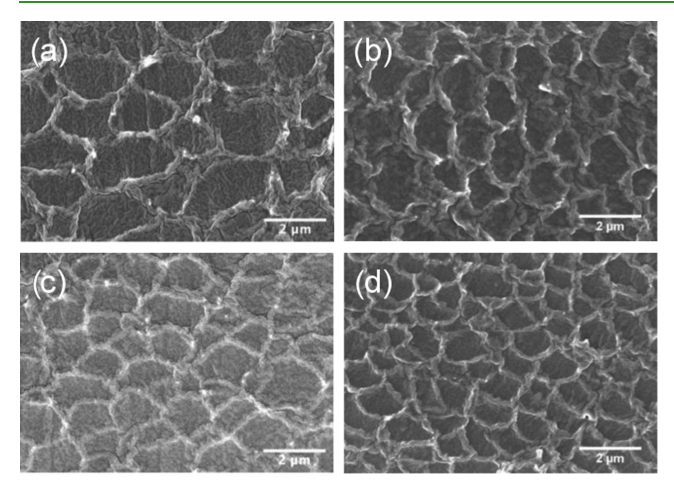


Figure 3. SEM images of the cross-sectional areas of latex composite films stabilized using (a) 2 wt % and (b) 3 wt % of *m*-CNC-hexyl-COOH and (c) 2 wt % and (d) 3 wt % of *MxG*-CNC-hexyl-COOH.

predominantly a polymer-only phase. Similar honeycomb-like network structures have also been observed before with Laponite and silica-stabilized latex films. Such excluded volume effect allows the CNCs to form percolating network structures at a much lower concentration than would be predicted in a composite where the filler is well dispersed and as such has an enhanced reinforcement effect. It is important to note that the SEM images of the cross-sectional area of the latex films stabilized with SDS do not reveal any such network structures (Figure S4).

A number of reports in the literature 48,58,59,69 have focused on accessing latex/CNC nanocomposites by taking advantage of noncovalent interactions between the CNCs and traditional surfactants and utilized surfactant and/or surfactant-coated CNCs as the stabilizers to access stable oil-in-water emulsions. Such latexes with the same monomer mixture but stabilized by a combination of CNC-COOH and SDS were prepared to compare their film properties to those of the alkyl-CNCs latex films. To this end, 2 wt % of m-CNC-COOH or MxG-CNC-COOH (with respect to (wrt) monomer) was dispersed in water along with SDS (10 mM, above CMC).⁴⁸ The monomer phase was then added, and the polymerization of emulsions was carried out using the same initiator systems to yield stable polymer latex particles with diameters of 172 \pm 10.5 nm (m-CNC-COOH/SDS) and 166 \pm 8.0 nm (MxG-CNC-COOH/ SDS) (Table S2). Nanocomposite films formed from the latexes stabilized with CNC-COOH/SDS (Figure S5) showed

a lower storage modulus in the rubber regime compared to CNC-hexyl-COOHs at the same CNC loadings (2 wt %) (Figures 4 and S6). The E' value of the m-CNC-COOH/SDSstabilized films at 60 °C is 11.2 ± 1.8 MPa (cf. 17.7 MPa for m-CNC-hexyl-COOH), while that of the MxG-CNC-COOH/ SDS-stabilized films at 60 °C is 12.7 \pm 1.6 MPa (cf. 25.9 MPa for MxG-CNC-hexyl-COOH). It is worth noting that SEM images of the CNC/SDS films (Figure S7) revealed no interconnected structures of the nanofillers. A possible explanation for the difference in microstructures is that the surface of the monomer droplets is predominantly stabilized with low-molecular-weight surfactants rather than the CNCs. Therefore, the coalescence and interfusion of latex particles during film formation does not lead to the formation of the honeycomb-like network structures compared to the latexes, which were covered only with CNCs. It is also possible that some of the SDS in the formulation coats the CNCs, making them more dispersible in the oil phase.

In addition to the mechanical properties, surfactant/CNC formulation may be expected to be more hydrophilic compared to the hexyl-functionalized CNC, which will affect the waterswelling behavior of the latex composite films. Indeed, latex films stabilized with CNC-COOH/SDS uptake more water relative to the hexyl-modified CNCs. The equilibrium water

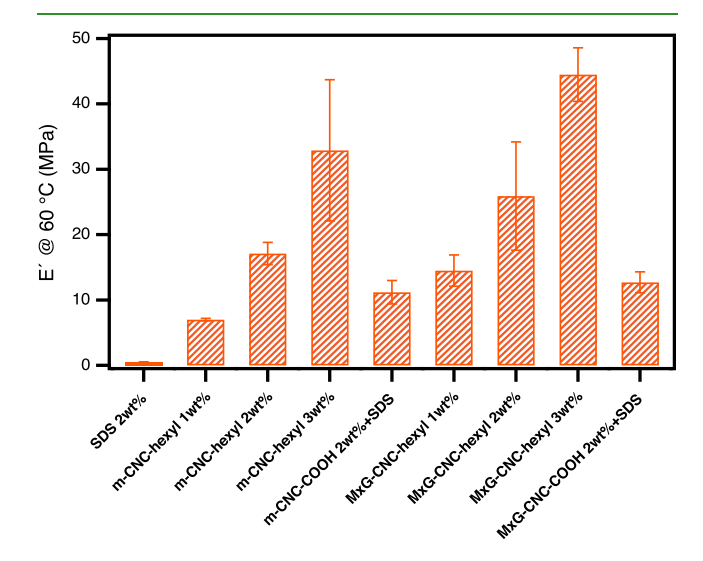


Figure 4. Comparison of the storage modulus (E') at 60 °C of as-cast latex composite films stabilized with various types and concentrations of stabilizers.

uptake is ca. 35 and 49 wt % for the latex films stabilized with m-CNC-COOH/SDS and MxG-CNC-COOH/SDS, respectively (Table S2), while the latex films containing CNC-hexyl-COOH only swell ca. 3 wt % for either m-CNC-hexyl-COOH or MxG-CNC-hexyl-COOHs. Such a reduction in water uptake offers advantages for the CNC-hexyl-COOH latex films, particularly in some coating formulations where water uptake generally leads to a reduction in the film property profile or coating effectiveness. 37,38

Effect of Microstructures on the Mechanical Properties. Since the above study suggests that the large reinforcement effect of the CNC/latex nanocomposites is attributed to the network structures formed by the latex templating effect, it is of interest to study how the mechanical properties will be affected if the microstructures are altered. To this end, the solution-cast films of the latex particles stabilized with alkyl-CNCs were melt-pressed at 90 °C with the goal of disrupting the preformed CNC honeycomb structure. The melt-pressed films appear homogeneous without any visible phase separation (Figure S8). A slight shrinkage in the film was observed on account of the elasticity of the polymer matrix, and this shrinkage was minimized in films with an increased amount of CNCs. SEM characterization was performed to investigate how the microstructures were affected by melt pressing. As can be seen from the SEM image of the crosssectional areas of the films (Figure 5a,b), the honeycomb network structure formed by the CNCs and latex particles has been significantly disrupted by the melt pressing process. The viscoelastic properties of the melt-pressed films were studied using DMA (Table 2). For the latex films containing only SDS

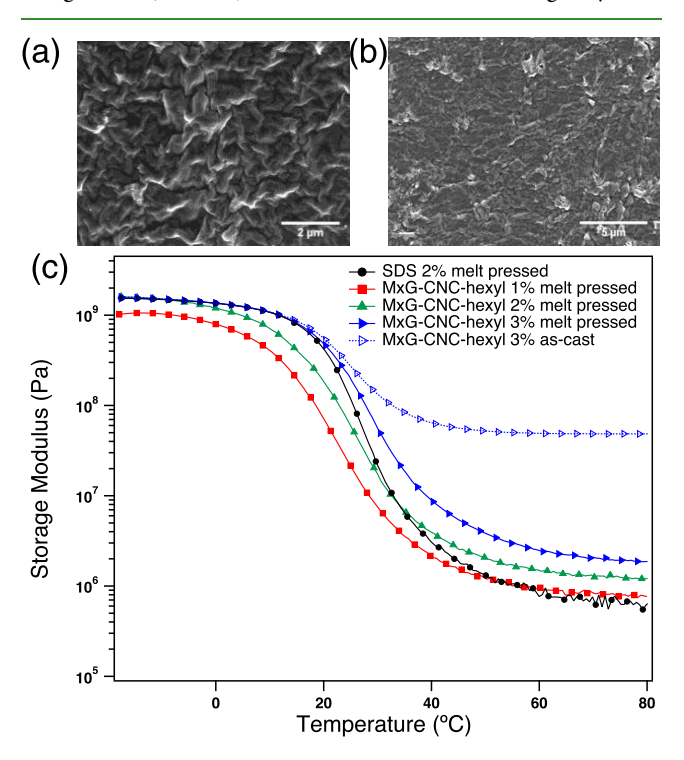


Figure 5. SEM images of the cross-sectional areas of melt-pressed latex composite films stabilized using (a) 3 wt % m-CNC-hexyl-COOH and (b) 3 wt % MxG-CNC-hexyl-COOH. (c) DMA temperature sweep study of the storage modulus (E') of the latex composite films stabilized with MxG-CNC-hexyl-COOH and SDS after melt pressing. Loss modulus (E'') and $\tan \delta$ peak are shown in SI (Figure S10).

as the stabilizer, the plateau storage modulus at 60 °C increased from (0.48 ± 0.05) to 0.76 MPa after melt pressing. The slight increase in storage modulus is presumably a consequence of the formation of a more compact structure within the films through melt pressing. On the other hand, the plateau storage modulus for the films stabilized with either m-CNC-hexyl-COOH (Figure S9) or MxG-CNC-hexyl-COOH (Figure 5c) both decreased dramatically as a result of the melt processing. It can be seen from the DMA results that the meltpressed films containing 1 wt % m-CNC-hexyl-COOH or MxG-CNC-hexyl-COOH now exhibit a similar storage modulus to the film containing SDS, which indicates that the nanofillers (at these loadings) now have a little to no reinforcement effect in these melt-pressed latex films. This result supports the hypothesis that the network structure of the CNCs formed by latex templating is key to the strong reinforcement effect observed in the solution-cast latex composite films, and a disruption of such network structure leads to a significant decrease in storage modulus of the meltpressed films.

Addition of CNC-COOH to the CNC-Hexyl-COOH-Stabilized Latexes. For nanocomposites containing rigid nanofillers, the mechanical reinforcement is also a function of the volume fraction of the rigid filler particles, but the relative modulus increase is greatly diminished upon reaching a higher filler content. In the case of the alkyl-CNCs latex composite films, a significant reinforcement effect is observed even at a relatively low filler content (1-3 wt %). Nonetheless, it was of interest to see whether the network can be further reinforced by increasing the CNC loading in the film. Since the ratio of monomer to aqueous phase is kept at 20:80 (w/w), one way to increase the CNC content relative to the monomer is to increase the CNC concentration in the aqueous phase. However, these hydrophobically functionalized CNCs have reduced dispersibility in the aqueous phase, and the viscosity of the CNC aqueous dispersion also increases rapidly as the CNC concentration increases, making it difficult to access stable oilin-water emulsions at a higher CNC content. Therefore, presynthesized latex particles stabilized with 3 wt % of m-CNC-hexyl-COOH or MxG-CNC-hexyl-COOH were mixed with a CNC-COOH aqueous dispersion (10 mg/mL) such that the total amount of CNC-COOH equals ca. 10 wt % wrt the monomer phase. After stirring the mixtures for 3 h, the latex suspensions were cast into composite films with a total CNC weight fraction of 13 wt %. Both latex composite films containing a higher concentration of m-CNC-COOH or MxG-CNC-COOH showed no visible phase separation; however, the films were more brittle at room temperature (for example, Figure S11 shows that there is cracking of these films around the cut edges). The mechanical properties of the latex composites were investigated by DMA, and the results showed that there is a significant increase in the modulus in the rubbery regime, with a storage modulus E' of 1040 \pm 31 and 988 \pm 23 MPa at 60 °C for the films stabilized with 13 wt % *m*-CNC and 13 wt % MxG-CNC, respectively (Figure 6a). The plateau modulus is more than 2000 times higher than the SDS latex films (without CNCs). It is also worth pointing out that the difference in storage modulus between films stabilized with m-CNCs and MxG-CNCs is not significant, suggesting that in these systems, the aspect ratio of individual nanocrystals becomes less important. Similar to the CNC latex films discussed above, the storage moduli of these 13 wt % composite films show a significant decrease in plateau modulus

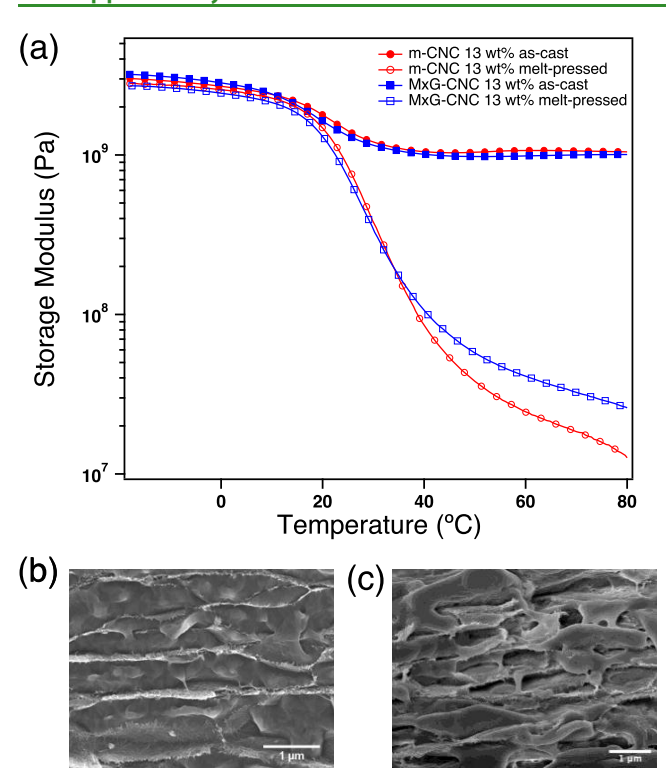


Figure 6. (a) Comparison of the storage moduli of as-cast and melt-pressed latex composite films stabilized with 13 wt % total of m-CNCs or MxG-CNCs. Loss modulus (E'') and $\tan \delta$ data are shown in the SI (Figure S12). SEM image of the cross-sectional areas of latex composite film stabilized with 13 wt % MxG-CNCs (b) as-cast and (c) after melt pressing.

after melt pressing. The E' value at 60 °C decreases to 25 \pm 7 and 39 \pm 14 MPa for the melt-pressed composites films containing 13 wt % of m-CNC and MxG-CNC, respectively. The large decrease in storage modulus is presumably also a consequence of the disruption of the network structures formed within the films as a result of the melt pressing.

With the goal of understanding the mechanical reinforcement effect, the internal structures of the latex composites stabilized with 13 wt % of MxG-CNCs were also investigated by SEM (Figure 6b). As shown in the SEM image of the crosssectional area of these films, a more layered microstructure (of what appears to be CNC-rich and polymer-rich layers) can be observed as opposed to the honeycomb network structure observed in films stabilized with 3 wt % of MxG-CNC-hexyl-COOH. The lack of any macroscopic phase separation suggests that the polymerized latex particles stabilized by hexyl-functionalized MxG-CNCs and the extra MxG-CNC-COOHs are compatibilized with each other during the ex situ aqueous mixing process. The higher reinforcement effect is again attributed to the formation of CNC network structures within the composite films by the latex templating effect. But in this case, the concentration of CNCs in the interstitial areas (the CNC-rich layers observed in SEM) is much higher compared to the network formed within the latex film stabilized with 3 wt % MxG-CNC-hexyl, which results in a further enhancement of the film's mechanical properties. Furthermore, the network structure could also be disrupted by melt pressing, as indicated by the SEM images of the meltpressed films (Figure 6c). This is consistent with the large decrease in storage modulus observed by DMA experiment

and is consistent with the previous study that the microstructures formed by the latex particles are crucial for the mechanical reinforcement of the nanocomposites.

CONCLUSIONS

Low-molecular-weight surfactant-free poly(St-co-EHA) latex particles with submicron sizes were successfully synthesized by miniemulsion polymerization using hexyl-modified CNCs as stabilizers. These latexes formed films that showed enhanced mechanical properties in the rubber regime relative to the films formed from SDS-stabilized latexes even at relative low CNC loadings (1 wt %). The strong mechanical reinforcement is attributed to the formation of CNC filler networks within the latex composite films as well as better interactions between alkyl-CNCs and polymer matrix on account of the in situ polymerization. The excluded volume of the latex particles results in the formation of a percolating honeycomb CNC-rich phase that reinforces the film even at low CNC concentrations. The disruption of this percolating CNC-rich network by melt pressing leads to a significant decrease in the mechanical properties of the films. Importantly, these alkyl-CNC-stabilized latexes were shown to form more mechanically robust films that also have lower water uptake than those prepared from the corresponding latexes stabilized with a combination of SDS and CNCs, highlighting some key advantages of being able to remove the low-molecular-weight surfactant from the formulation. Finally, it was also shown that the mechanical properties of the latex composite films can be further enhanced by the addition of CNC-COOHs to the presynthesized CNCstabilized latexes. The ability of using alkyl-modified CNCs to access latex films without the need of a low-molecular-weight surfactant to access films with enhanced mechanical properties (even at low CNC loading) and reduced water uptake makes these CNCs an attractive option as a combined green surfactant and reinforcing agent in coating and adhesive applications.

ASSOCIATED CONTENT

Supporting Information

The Supporting Information is available free of charge at https://pubs.acs.org/doi/10.1021/acsapm.0c00263.

Percolation model; latex particle coverage calculation; AFM height images of m-CNC-COOH and MxG-CNC-COOH; FTIR spectra of oxidized and hexyl-modified m-CNC-hexyl-COOH and MxG-CNC-hexyl-COOH; elemental analysis and ζ potential of functionalized CNCs; loss modulus and $\tan \delta$ of the latex films stabilized with SDS or hexyl CNCs; SEM images of the cross-sectional areas of latex films stabilized with SDS; photographs of latex composite films stabilized with SDS-coated CNC-COOH; comparison of the size of latex parties, mechanical properties and water swelling of the latex composite films stabilized with CNC-hexyl and SDS/ CNC-COOH; DMA temperature sweep study of the latex composite films stabilized with CNC-hexyl and SDS/CNC-COOH; SEM images of the cross-sectional areas of latex films stabilized with SDS/m-CNC-COOH and SDS/MxG-CNC-COOH; photographs of meltpressed latex composite films stabilized with CNChexyl-COOH; DMA temperature sweep study of the latex films stabilized with SDS or m-CNC-hexyl-COOH after melt pressing; photographs of latex composite films

contain 13 wt % of m-CNC and MxG-CNC; and loss modulus and $\tan \delta$ of the latex films stabilized with 13 wt % of m-CNC and MxG-CNC (PDF)

AUTHOR INFORMATION

Corresponding Author

Stuart J. Rowan — Pritzker School of Molecular Engineering and Department of Chemistry, University of Chicago, Chicago, Illinois 60637, United States; Chemical and Engineering Sciences, Argonne National Laboratory, Lemont, Illinois 60439, United States; orcid.org/0000-0001-8176-0594; Email: stuartrowan@uchicago.edu

Authors

Yefei Zhang — Pritzker School of Molecular Engineering, University of Chicago, Chicago, Illinois 60637, United States Han Yang — Pritzker School of Molecular Engineering, University of Chicago, Chicago, Illinois 60637, United States; orcid.org/0000-0003-3971-1734

Nevin Naren — Pritzker School of Molecular Engineering, University of Chicago, Chicago, Illinois 60637, United States

Complete contact information is available at: https://pubs.acs.org/10.1021/acsapm.0c00263

Notes

The authors declare the following competing financial interest(s): Part of this work is included in and expands on the following patent application: Rowan, S. J.; Zhang, Y. Nano-Emulsion and Nano-Latexes With Functionalized Cellulose Nanocrystals. Patent Application No. US 15/770,880, April 2018. This work reported here goes into much more detail than the patent application and there is a significant amount of new work outlined in this paper.

ACKNOWLEDGMENTS

This project was supported by the National Science Foundation under grant no. NSF #1204948, the National Science Foundation PIRE program under grant no. NSF #1743475, the Sherwin-Williams company, and the Pritzker School of Molecular Engineering at the University of Chicago. Part of this work was carried out using the Soft Matter Characterization Facility of the University of Chicago. SEM characterization was carried out at the Chicago MRSEC center (funded by NSF DMR-1420709). The authors thank Aloterra Energy LLC for the donation of *MxG* stalks.

■ REFERENCES

- (1) DeFusco, A. J.; Sehgal, K. C.; Bassett, D. R. Overview of Uses of Polymer Latexes. *Polymeric Dispersions: Principles and Applications*; Springer: Netherlands, Dordrecht, 1997; pp 379–396.
- (2) Steward, P. A.; Hearn, J.; Wilkinson, M. C. Overview of Polymer Latex Film Formation and Properties. *Adv. Colloid Interface Sci.* **2000**, 86, 195–267.
- (3) Winnik, M. A. Latex Film Formation. Curr. Opin. Colloid Interface Sci. 1997, 2, 192-199.
- (4) Xiong, M.; Wu, L.; Zhou, S.; You, B. Preparation and Characterization of Acrylic Latex/Nano-SiO₂ Composites. *Polym. Int.* **2002**, *51*, 693–698.
- (5) Kaboorani, A.; Riedl, B. Nano-Aluminum Oxide as a Reinforcing Material for Thermoplastic Adhesives. *J. Ind. Eng. Chem.* **2012**, *18*, 1076–1081.
- (6) Zhou, S.; Wu, L.; Xiong, M.; He, Q.; Chen, G. Dispersion and UV–VIS Properties of Nanoparticles in Coatings. *J. Dispers. Sci. Technol.* **2005**, 25, 417–433.

- (7) Xiong, M.; Gu, G.; You, B.; Wu, L. Preparation and Characterization of Poly(Styrene Butylacrylate) Latex/Nano-ZnO Nanocomposites. *J. Appl. Polym. Sci.* **2003**, *90*, 1923–1931.
- (8) Kajtna, J.; Šebenik, U. Microsphere Pressure Sensitive Adhesives—Acrylic Polymer/Montmorillonite Clay Nanocomposite Materials. *Int. J. Adhes. Adhes.* **2009**, *29*, 543–550.
- (9) Dufresne, A.; Paillet, M.; Putaux, J. L.; Canet, R.; Carmona, F.; Delhaes, P.; Cui, S. Processing and Characterization of Carbon Nanotube/Poly(Styrene-Co-Butyl Acrylate) Nanocomposites. *J. Mater. Sci.* **2002**, *37*, 3915–3923.
- (10) Ouzas, A.; Niinivaara, E.; Cranston, E. D.; Dubé, M. A. In Situ Semibatch Emulsion Polymerization of 2-Ethyl Hexyl Acrylate/n-Butyl Acrylate/Methyl Methacrylate/Cellulose Nanocrystal Nanocomposites for Adhesive Applications. *Macromol. React. Eng.* **2018**, *12*, No. 1700068.
- (11) Mabrouk, A. B.; Dufresne, A.; Boufi, S. Cellulose Nanocrystal as Ecofriendly Stabilizer for Emulsion Polymerization and Its Application for Waterborne Adhesive. *Carbohydr. Polym.* **2020**, 229, No. 115504.
- (12) Trovatti, E.; Oliveira, L.; Freire, C. S. R.; Silvestre, A. J. D.; Pascoal Neto, C.; Cruz Pinto, J. J. C.; Gandini, A. Novel Bacterial Cellulose—Acrylic Resin Nanocomposites. *Compos. Sci. Technol.* **2010**, 70, 1148–1153.
- (13) Pu, Y.; Zhang, J.; Elder, T.; Deng, Y.; Gatenholm, P.; Ragauskas, A. J. Investigation into Nanocellulosics versus Acacia Reinforced Acrylic Films. *Composites, Part B* **2007**, *38*, 360–366.
- (14) Elmabrouk, A.; Wim, T.; Dufresne, A.; Boufi, S. Preparation of Poly(Styrene-co-Hexylacrylate)/Cellulose Whiskers Nanocomposites via Miniemulsion Polymerization. *J. Appl. Polym. Sci.* **2009**, *114*, 2946–2955.
- (15) Dastjerdi, Z.; Cranston, E. D.; Berry, R.; Fraschini, C.; Dubé, M. A. Polymer Nanocomposites for Emulsion-Based Coatings and Adhesives. *Macromol. React. Eng.* **2019**, *13*, No. 1800050.
- (16) Dufresne, A. Cellulose Nanomaterials as Green Nanoreinforcements for Polymer Nanocomposites. *Philos. Trans. R. Soc., A* **2018**, 376, No. 20170040.
- (17) Moon, R. J.; Martini, A.; Nairn, J.; Simonsen, J.; Youngblood, J. Cellulose Nanomaterials Review: Structure, Properties and Nanocomposites. *Chem. Soc. Rev.* **2011**, *40*, 3941.
- (18) Eichhorn, S. J.; Dufresne, A.; Aranguren, M.; Marcovich, N. E.; Capadona, J. R.; Rowan, S. J.; Weder, C.; Thielemans, W.; Roman, M.; Renneckar, S.; Gindl, W.; Veigel, S.; Keckes, J.; Yano, H.; Abe, K.; Nogi, M.; Nakagaito, A. N.; Mangalam, A.; Simonsen, J.; Benight, A. S.; Bismarck, A.; Berglund, L. A.; Peijs, T. Review: Current International Research into Cellulose Nanofibres and Nanocomposites. *J. Mater. Sci.* 2010, 45, 1–33.
- (19) Habibi, Y.; Lucia, L. A.; Rojas, O. J. Cellulose Nanocrystals: Chemistry, Self-Assembly, and Applications. *Chem. Rev.* **2010**, *110*, 3479–3500.
- (20) Capadona, J. R.; Shanmuganathan, K.; Tyler, D. J.; Rowan, S. J.; Weder, C. Stimuli-Responsive Polymer Nanocomposites Inspired by the Sea Cucumber Dermis. *Science* **2008**, *319*, 1370–1374.
- (21) Dagnon, K. L.; Shanmuganathan, K.; Weder, C.; Rowan, S. J. Water-Triggered Modulus Changes of Cellulose Nanofiber Nanocomposites with Hydrophobic Polymer Matrices. *Macromolecules* **2012**, *45*, 4707–4715.
- (22) Shanmuganathan, K.; Capadona, J. R.; Rowan, S. J.; Weder, C. Biomimetic Mechanically Adaptive Nanocomposites. *Prog. Polym. Sci.* **2010**, *35*, 212–222.
- (23) Jorfi, M.; Roberts, M. N.; Foster, E. J.; Weder, C. Physiologically Responsive, Mechanically Adaptive Bio-Nanocomposites for Biomedical Applications. *ACS Appl. Mater. Interfaces* **2013**, *5*, 1517–1526.
- (24) Kargarzadeh, H.; Mariano, M.; Huang, J.; Lin, N.; Ahmad, I.; Dufresne, A.; Thomas, S. Recent Developments on Nanocellulose Reinforced Polymer Nanocomposites: A Review. *Polymer* **2017**, 368–393.

- (25) Calvino, C.; Macke, N.; Kato, R.; Rowan, S. J. Development, Processing and Applications of Bio-Sourced Cellulose Nanocrystal Composites. *Prog. Polym. Sci.* **2020**, No. 101221.
- (26) Favier, V.; Canova, G. R.; Cavaillé, J. Y.; Chanzy, H.; Dufresne, A.; Gauthier, C. Nanocomposite Materials from Latex and Cellulose Whiskers. *Polym. Adv. Technol.* **1995**, *6*, 351–355.
- (27) Favier, V.; Chanzy, H.; Cavaillé, J. Y. Polymer Nanocomposites Reinforced by Cellulose Whiskers. *Macromolecules* **1995**, 28, 6365–6367.
- (28) Favier, V.; Cavaille, J. Y.; Canova, G. R.; Shrivastava, S. C. Mechanical Percolation in Cellulose Whisker Nanocomposites. *Polym. Eng. Sci.* **1997**, 37, 1732–1739.
- (29) Hajji, P.; Cavaillé, J. Y.; Favier, V.; Gauthier, C.; Vigier, G. Tensile Behavior of Nanocomposites from Latex and Cellulose Whiskers. *Polym. Compos.* **1996**, *17*, 612–619.
- (30) Helbert, W.; Cavaillé, J. Y.; Dufresne, A. Thermoplastic Nanocomposites Filled with Wheat Straw Cellulose Whiskers. Part I: Processing and Mechanical Behavior. *Polym. Compos.* **1996**, *17*, 604–611.
- (31) Dufresne, A.; Cavaillé, J.-Y.; Helbert, W. Thermoplastic Nanocomposites Filled with Wheat Straw Cellulose Whiskers. Part II: Effect of Processing and Modeling. *Polym. Compos.* **1997**, *18*, 198–210.
- (32) Dubief, D.; Samain, E.; Dufresne, A. Polysaccharide Microcrystals Reinforced Amorphous Poly(β -Hydroxyoctanoate) Nanocomposite Materials. *Macromolecules* **1999**, *32*, 5765–5771.
- (33) Annamalai, P. K.; Dagnon, K. L.; Monemian, S.; Foster, E. J.; Rowan, S. J.; Weder, C. Water-Responsive Mechanically Adaptive Nanocomposites Based on Styrene–Butadiene Rubber and Cellulose Nanocrystals—Processing Matters. ACS Appl. Mater. Interfaces 2014, 6, 967–976.
- (34) Tkalya, E.; Ghislandi, M.; Thielemans, W.; Van Der Schoot, P.; De With, G.; Koning, C. Cellulose Nanowhiskers Templating in Conductive Polymer Nanocomposites Reduces Electrical Percolation Threshold 5-Fold. ACS Macro Lett. 2013, 2, 157–163.
- (35) Limousin, E.; Rafaniello, I.; Schäfer, T.; Ballard, N.; Asua, J. M. Linking Film Structure and Mechanical Properties in Nanocomposite Films Formed from Dispersions of Cellulose Nanocrystals and Acrylic Latexes. *Langmuir* **2020**, *36*, 2052–2062.
- (36) Keddie, J. Film Formation of Latex. *Mater. Sci. Eng., R* **1997**, 21, 101–170.
- (37) Gundabala, V. R.; Lei, C.; Ouzineb, K.; Dupont, O.; Keddie, J. L.; Routh, A. F. Lateral Surface Nonuniformities in Drying Latex Films. *AIChE J.* **2008**, *54*, 3092–3105.
- (38) Yang, Y.-K.; Li, H.; Wang, F. Studies on the Water Resistance of Acrylic Emulsion Pressure-Sensitive Adhesives (PSAs). *J. Adhes. Sci. Technol.* **2003**, *17*, 1741–1750.
- (39) Limousin, E.; Ballard, N.; Asua, J. M. Synthesis of Cellulose Nanocrystal Armored Latex Particles for Mechanically Strong Nanocomposite Films. *Polym. Chem.* **2019**, *10*, 1823–1831.
- (40) Errezma, M.; Mabrouk, A. B.; Magnin, A.; Dufresne, A.; Boufi, S. Surfactant-Free Emulsion Pickering Polymerization Stabilized by Aldehyde-Functionalized Cellulose Nanocrystals. *Carbohydr. Polym.* **2018**, 202, 621–630.
- (41) Kalashnikova, I.; Bizot, H.; Cathala, B.; Capron, I. New Pickering Emulsions Stabilized by Bacterial Cellulose Nanocrystals. *Langmuir* **2011**, *27*, 7471–7479.
- (42) Kalashnikova, I.; Bizot, H.; Bertoncini, P.; Cathala, B.; Capron, I. Cellulosic Nanorods of Various Aspect Ratios for Oil in Water Pickering Emulsions. *Soft Matter* **2013**, *9*, 952–959.
- (43) Kalashnikova, I.; Bizot, H.; Cathala, B.; Capron, I. Modulation of Cellulose Nanocrystals Amphiphilic Properties to Stabilize Oil/Water Interface. *Biomacromolecules* **2012**, *13*, 267–275.
- (44) Tang, J.; Lin, N.; Zhang, Z.; Pan, C.; Yu, G. Nanopolysaccharides in Emulsion Stabilization; Springer: Singapore, 2019; pp 221-254.
- (45) Jiménez Saelices, C.; Capron, I. Design of Pickering Micro- and Nanoemulsions Based on the Structural Characteristics of Nanocelluloses. *Biomacromolecules* **2018**, *19*, 460–469.

- (46) Jiménez Saelices, C.; Save, M.; Capron, I. Synthesis of Latex Stabilized by Unmodified Cellulose Nanocrystals: The Effect of Monomers on Particle Size. *Polym. Chem.* **2019**, *10*, 727–737.
- (47) Bai, L.; Lv, S.; Xiang, W.; Huan, S.; McClements, D. J.; Rojas, O. J. Oil-in-Water Pickering Emulsions via Microfluidization with Cellulose Nanocrystals: 1. Formation and Stability. *Food Hydrocolloids* **2019**, *96*, 699–708.
- (48) Kedzior, S. A.; Marway, H. S.; Cranston, E. D. Tailoring Cellulose Nanocrystal and Surfactant Behavior in Miniemulsion Polymerization. *Macromolecules* **2017**, *50*, 2645–2655.
- (49) Kedzior, S. A.; Kiriakou, M.; Niinivaara, E.; Dubé, M. A.; Fraschini, C.; Berry, R. M.; Cranston, E. D. Incorporating Cellulose Nanocrystals into the Core of Polymer Latex Particles via Polymer Grafting. ACS Macro Lett. 2018, 7, 990–996.
- (50) Zhang, Y.; Karimkhani, V.; Makowski, B. T.; Samaranayake, G.; Rowan, S. J. Nanoemulsions and Nanolatexes Stabilized by Hydrophobically Functionalized Cellulose Nanocrystals. *Macromolecules* **2017**, *50*, 6032–6042.
- (51) Werner, A.; Schmitt, V.; Sèbe, G.; Héroguez, V. Synthesis of Surfactant-Free Micro-and Nanolatexes from Pickering Emulsions Stabilized by Acetylated Cellulose Nanocrystals. *Polym. Chem.* **2017**, *8*, 6064–6072.
- (52) Tang, C.; Chen, Y.; Luo, J.; Low, M. Y.; Shi, Z.; Tang, J.; Zhang, Z.; Peng, B.; Tam, K. C. Pickering Emulsions Stabilized by Hydrophobically Modified Nanocellulose Containing Various Structural Characteristics. *Cellulose* **2019**, *26*, 7753–7767.
- (53) Zhou, J.; Li, Y.; Li, H.; Yao, H. Cellulose Nanocrystals/ Fluorinated Polyacrylate Soap-Free Emulsion Prepared via RAFT-Assisted Pickering Emulsion Polymerization. *Colloids Surf., B* **2019**, 177. 321–328.
- (54) Bertsch, P.; Fischer, P. Adsorption and Interfacial Structure of Nanocelluloses at Fluid Interfaces. *Adv. Colloid Interface Sci.* **2020**, 276, No. 102089.
- (55) Bai, L.; Greca, L. G.; Xiang, W.; Lehtonen, J.; Huan, S.; Nugroho, R. W. N.; Tardy, B. L.; Rojas, O. J. Adsorption and Assembly of Cellulosic and Lignin Colloids at Oil/Water Interfaces. *Langmuir* **2019**, *35*, 571–588.
- (56) Bai, L.; Xiang, W.; Huan, S.; Rojas, O. J. Formulation and Stabilization of Concentrated Edible Oil-in-Water Emulsions Based on Electrostatic Complexes of a Food-Grade Cationic Surfactant (Ethyl Lauroyl Arginate) and Cellulose Nanocrystals. *Biomacromolecules* 2018, 19, 1674–1685.
- (57) Nigmatullin, R.; Johns, M. A.; Muñoz-García, J. C.; Gabrielli, V.; Schmitt, J.; Angulo, J.; Khimyak, Y. Z.; Scott, J. L.; Edler, K. J.; Eichhorn, S. J. Hydrophobization of Cellulose Nanocrystals for Aqueous Colloidal Suspensions and Gels. *Biomacromolecules* **2020**, 1812.
- (58) Dastjerdi, Z.; Cranston, E. D.; Dubé, M. A. Synthesis of Poly(n-Butyl Acrylate/Methyl Methacrylate)/CNC Latex Nanocomposites via In Situ Emulsion Polymerization. *Macromol. React. Eng.* **2017**, *11*, No. 1700013.
- (59) Dastjerdi, Z.; Cranston, E. D.; Dubé, M. A. Pressure Sensitive Adhesive Property Modification Using Cellulose Nanocrystals. *Int. J. Adhes. Adhes.* 2018, 81, 36–42.
- (60) Ben Mabrouk, A.; Kaddami, H.; Magnin, A.; Belgacem, M. N.; Dufresne, A.; Boufi, S. Preparation of Nanocomposite Dispersions Based on Cellulose Whiskers and Acrylic Copolymer by Miniemulsion Polymerization: Effect of the Silane Content. *Polym. Eng. Sci.* **2011**, *51*, 62–70.
- (61) Haaj, S. B.; Thielemans, W.; Magnin, A.; Boufi, S. Starch Nanocrystal Stabilized Pickering Emulsion Polymerization for Nanocomposites with Improved Performance. *ACS Appl. Mater. Interfaces* **2014**, *6*, 8263–8273.
- (62) Cudjoe, E.; Hunsen, M.; Xue, Z.; Way, A. E.; Barrios, E.; Olson, R. A.; Hore, M. J. A.; Rowan, S. J. Miscanthus Giganteus: A Commercially Viable Sustainable Source of Cellulose Nanocrystals. *Carbohydr. Polym.* **2017**, *155*, 230–241.
- (63) Kang, K.; Kan, C.; Du, Y.; Liu, D. Synthesis and Properties of Soap-Free Poly(Methyl Methacrylate-Ethyl Acrylate-Methacrylic

- Acid) Latex Particles Prepared by Seeded Emulsion Polymerization. Eur. Polym. J. 2005, 41, 439–445.
- (64) Capadona, J. R.; Shanmuganathan, K.; Trittschuh, S.; Seidel, S.; Rowan, S. J.; Weder, C. Polymer Nanocomposites with Nanowhiskers Isolated from Microcrystalline Cellulose. *Biomacromolecules* **2009**, *10*, 712–716.
- (65) Yang, H.; Zhang, Y.; Kato, R.; Rowan, S. J. Preparation of Cellulose Nanofibers from Miscanthus x. Giganteus by Ammonium Persulfate Oxidation. *Carbohydr. Polym.* **2019**, 212, 30–39.
- (66) Ouali, N.; Cavaille, J. Y.; Perez, J. Elastic, Viscoelastic and Plastic Behavior of Multiphase Polymer Blends. *Plast., Rubber Compos. Process. Appl.* **1991**, *16*, 55–60.
- (67) González-Matheus, K.; Leal, G. P.; Asua, J. M. Film Formation from Pickering Stabilized Waterborne Polymer Dispersions. *Polymer* **2015**, *69*, 73–82.
- (68) Negrete-Herrera, N.; Putaux, J.-L.; David, L.; De Haas, F.; Bourgeat-Lami, E. Polymer/Laponite Composite Latexes: Particle Morphology, Film Microstructure, and Properties. *Macromol. Rapid Commun.* **2007**, 28, 1567–1573.
- (69) Bai, L.; Xiang, W.; Huan, S.; Rojas, O. J. Formulation and Stabilization of Concentrated Edible Oil-in-Water Emulsions Based on Electrostatic Complexes of a Food-Grade Cationic Surfactant (Ethyl Lauroyl Arginate) and Cellulose Nanocrystals. *Biomacromolecules* 2018, 19, 1674–1685.